Surface & Coatings Technology 325 (2017) 98–106

Contents lists available at ScienceDirect

Surface & Coatings Technology

journal homepage: www.elsevier.com/locate/surfcoat

High temperature erosion behavior of plasma sprayed NiCrAlY/WC-Co/cenosphere coating

Mahantayya Mathapati *, M.R. Ramesh, Mrityunjay Doddamani

Department of Mechanical Engineering, National Institute of Technology Karnataka, Surathkal, India

ARTICLE INFO

Article history:
Received 12 March 2017
Revised 19 May 2017
Accepted in revised form 13 June 2017
Available online 15 June 2017

Keywords:
Plasma spray
Cenospheres
Erosion
Brittle failure

ABSTRACT

High temperature erosive behavior of plasma sprayed NiCrAlY-25WC-Co/cenosphere coating deposited on MDN 321 steel is investigated in the present work. Coating is characterized using Scanning Electron Microscopy (SEM) and X-Ray Diffraction (XRD). Microhardness, porosity, adhesion strength, fracture toughness and ductility of the coating are quantified. Solid particle erosion test is conducted at 200, 400 and 600 °C with 30 and 90° impact angles using alumina erodent. Optical profilometer is used to evaluate erosion volume loss. Erosion resistance of the coating is observed to be higher than the substrate for the test temperatures chosen and noted to be more prominent at lower impact angle and higher temperature. High temperature stability of mullite, alumina and oxide layer assists in increasing erosion resistance of coating. The eroded coating surface morphology reveals the brittle mode of material removal.

© 2017 Elsevier B.V. All rights reserved.

1. Introduction

Erosion is the material removal phenomena resulting from solid particles impingement on target surface. It becomes trivial and complex to address erosion in components working at elevated temperature like in gas and steam turbines, jet engine parts, coal-fired power plant boiler tubes etc. [1]. Alloys of nickel and stainless steel used in these components provide good mechanical strength. Nevertheless, they lack better erosion, wear and corrosion resistance leading to reduced service life [2]. Erosive resistance of such components can be enhanced by suitable surface modification technique like thermal spray coatings [3–6]. Among available thermal spray coatings, plasma spray is extensively used for wear resistance applications [7–9]. With the available MCrAlY based coatings, NiCrAlY is widely used for oxidation, corrosion and wear resistance applications [10–13]. However, these coatings find industry limitations due to lower hardness compared to carbides, ceramics and oxides [14]. Nevertheless, erosion resistance of these coatings can be significantly improved by reinforcing the hard phases like WC, Al_2O_3, Cr_3C_2, Cr_2O_3, TiC, TiO, SiC, TiN, CeO_2, ZrO_2 etc. [15]. WC-Co possesses higher hardness, better ductility, chemical inertness and lower frictional values compared to Cr_3C_2. These properties improve the wear resistance of WC-Co coatings [16] and might enhance erosion resistance in NiCrAlY. However, NiCrAlY and WC-Co powders are expensive, limiting wide adaptability for various structural components. Usage of industrial wastes like fly ash cenospheres which are available in abundance and are inexpensive can be promising constituent material in such coatings.

Fly ash is a by-product produced due to combustion of coal in thermal power plant. These are spherical in shape, inexpensive, readily available in powder form and possesses superior mechanical properties [17]. Fly ash consist mainly of oxides of silicon (SiO_2), aluminium (Al_2O_3), iron (Fe_2O_3) and mullite ($3Al_2O_3.2SiO_2$). Among them aluminium oxide and mullite possess high temperature stability, wear, erosion and corrosion resistance [18,19]. These properties can be exploited well if fly ash is used in coatings. Several researchers studied the feasibility of fly ash as coating material. Mishra et al. [20] investigated the suitability of fly ash as feedstock using plasma spray approach. Rama Krishna et al. [21] studied the hardness and sliding wear behavior of fly ash coating deposited using detonation spray technique on mild steel. They reported that fly ash coating has better hardness and coefficient of friction compared to mild steel. Sidhu et al. [22] estimated wear, oxidation and salt corrosion behavior of plasma sprayed fly ash coating. Their study reveals that fly ash coating exhibits better oxidation and salt corrosion resistance as compared to carbon steel substrate. Effect of plasma torch power levels on erosion behavior of plasma sprayed fly ash premixed with aluminium is presented by Sahu et al. [23]. Addition of aluminium increases the erosion resistance of the coating is reported in their study. Behera and Mishra [24] studied the plasma sprayed fly ash composite coating mixed with quartz and illmenite on copper substrate and results reveal better interfacial adhesion between substrate and coating. In recent past, very few studies are available on fly ash composite coatings. However, they lack in high temperature erosion response of fly ash coatings. This fact necessitates study of elevated temperature erosion behavior of proposed NiCrAlY-25WC-Co/Fly ash

* Corresponding author.
E-mail address: mahantkm.me14f09@nitk.edu.in (M. Mathapati).

http://dx.doi.org/10.1016/j.surfcoat.2017.06.033
0257-8972/© 2017 Elsevier B.V. All rights reserved.

Table 1
Chemical composition of the substrate[a].

Element	wt%
C	0.10
Mn	1.46
Cr	18.13
Ni	10.36
Ti	0.62
Si	0.55
Fe	Bal

[a] As provided by MIDHANI, Hyderabad, India.

cenosphere coating. Furthermore, understanding the mechanism of hollow cenospheres in erosive behavior of NiCrAlY-25WC-Co coating is an interesting and challenging task. Usage of such environmental pollutants in coatings might further reduce landfill burden and if developed successfully are eco-friendly.

In the present investigation, NiCrAlY-25WC-Co/Fly ash cenosphere coating is deposited on MDN 321 steel substrate using atmospheric plasma spray process. Further, samples are subjected to microstructural characterisation. Erosion behavior of coating and substrate is investigated at 200, 400, and 600 °C with 30 and 90° impingement angles using Al_2O_3 erodent. Weight loss and volume loss methods are used to estimate erosion loss. Erosion mechanism is discussed using SEM and EDS.

2. Materials and methods

2.1. Materials

MDN 321 steel procured from Mishra Dhatu Nigam Ltd., Hyderabad, India is used as substrate. Table 1 presents chemical composition of MDN 321 steel substrate. Substrate is cut to the dimension of 25 × 20 × 4 mm prior to plasma spraying. Commercially available gas atomised NiCrAlY, agglomerated and sintered WC-Co powders and fly ash cenospheres are used as coating feedstock. The nominal particle size distributions of powders are measured by laser diffraction technique (Cilas 1064, France) while density is measured using pycnometer and the values are reported in Table 2. These powders are blended mechanically with mass fraction of NiCrAlY-25WC-Co and 30% cenospheres before getting sprayed. Fig. 1 presents micrograph of as blended powder mix. Uniform dispersion of cenospheres in NiCrAlY-25WC-Co network is clearly evident from the micrograph affirming suitability and feasibility of the mechanical blending adopted.

2.2. Coating deposition

NiCrAlY-25WC-Co and cenospheres blend is deposited by atmospheric plasma spray process using METCO USA 3 MB equipment (M/s. Spraymet Surface Technologies Pvt. Ltd., Bangalore, India). Before spraying, substrate is grit blasted using alumina powder of 150 μm size to promote better adhesion between the coating and substrate. Details of spray parameters are listed in Table 3. During plasma spraying, powder is supplied by the feeder is mixed with argon gas flowing from

Table 2
Particle size (μm) distribution and density of powders.

Particle size	NiCrAlY	WC/Co	Cenospheres[a]
D(0.1)	41.88	23.52	–
D(0.5)	70.75	38.78	–
D(0.9)	120.33	64.11	–
0–10%	–	–	106
70–90%	–	–	63
0–30%	–	–	53
Mean	76.54	41.71	65.00
Density (g/cm^3)	4.18	10.60	0.85

[a] As specified by Cenosphere India Pvt. Ltd., Kolkata, India.

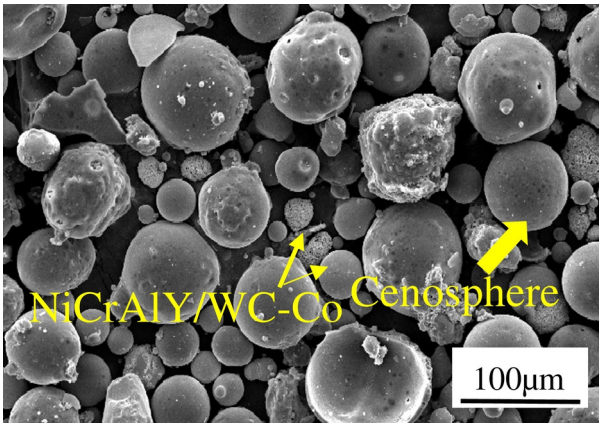

Fig. 1. Morphology of as blended NiCrAlY/WC-Co and fly ash cenopsheres.

compressor at chosen pressure. This mixture flows towards the plasma stream and get deposits on the substrate. Deposition of coating per pass is in the range of 12–15 μm having 40–45% spraying efficiency. Thickness of the developed coating is quantified through SEM. Porosity of coating is computed using optical microscope supported with Biovis image analyser (ARTRAY, AT 130, JAPAN). Twenty field views are analysed and average values are reported. Phases in powder and coating are analysed using (DX GE-2P, JEOL, JAPAN) X-ray diffractometer.

2.3. Adhesion strength and indentation fracture toughness

Adhesion strength of coating is estimated through pull-off test as outlined in ASTM C-633-13. Test is carried out in tension mode with

Table 3
Plasma spray process parameters[a].

Plasma gas (Argon + Hydrogen)	Pressure	0.75 MPa
	flow	150 lpm
Powder feed gas (Argon)	Pressure	0.35 MPa
	Flow	6 lpm
Current		1350 A
Voltage		60–70 V
Powder feed rate		120 g/min
Stand of distance		100–125 mm

[a] As provided by Spraymet Surface Technologies Pvt. Ltd., Bangalore, India.

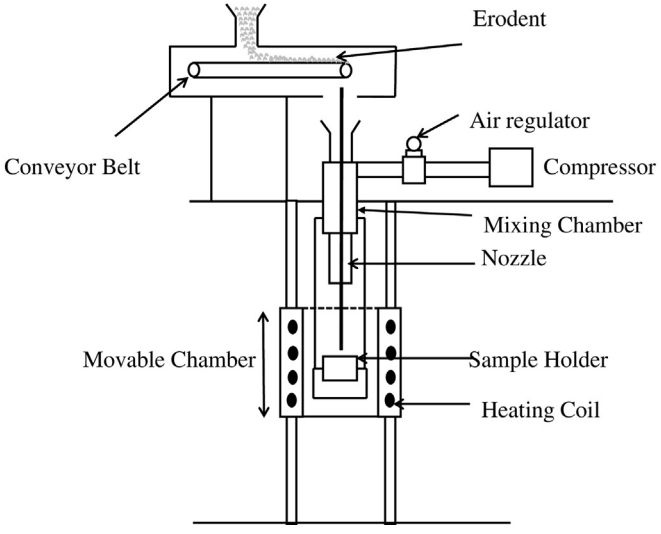

Fig. 2. Schematic representation of the erosion test setup.

Table 4
Erosion test parameters.

Erodent	Alumina
Erodent average size (μm)	50
Particle velocity (m/s)	30
Erodent feed rate (g/min)	2
Impact angle (degree)	30 and 90
Temperature (°C)	200,400 and 600
Test time (min)	15
Standoff distance (mm)	10
Nozzle diameter (mm)	1.5

strain rate of 0.5 mm/min using Universal Testing Machine (Shimadzu hydraulic tensile machine, AG-X Plus, JAPAN). The cylindrical sample of dimension 25 × 25 mm is used for the adhesion strength test. HTK Ultra bond epoxy resin is used as an adhesive to glue NiCrAlY-25WC-Co/cenosphere coated sample with the counter block and is cured at 150 °C for 3 h in tubular furnace (Heatron Industrial Heaters, INDIA). The adhesion strength is computed by taking ratio of maximum load to cross sectional area and average values of five replicates are reported.

Fracture toughness of developed coating is estimated by indentation method. Indentation is carried out using Vickers pyramid indenter in such a way that indenter diagonal is parallel to coating-substrate interface with 1 kg load and 15 s dwell time [25]. Fracture toughness is

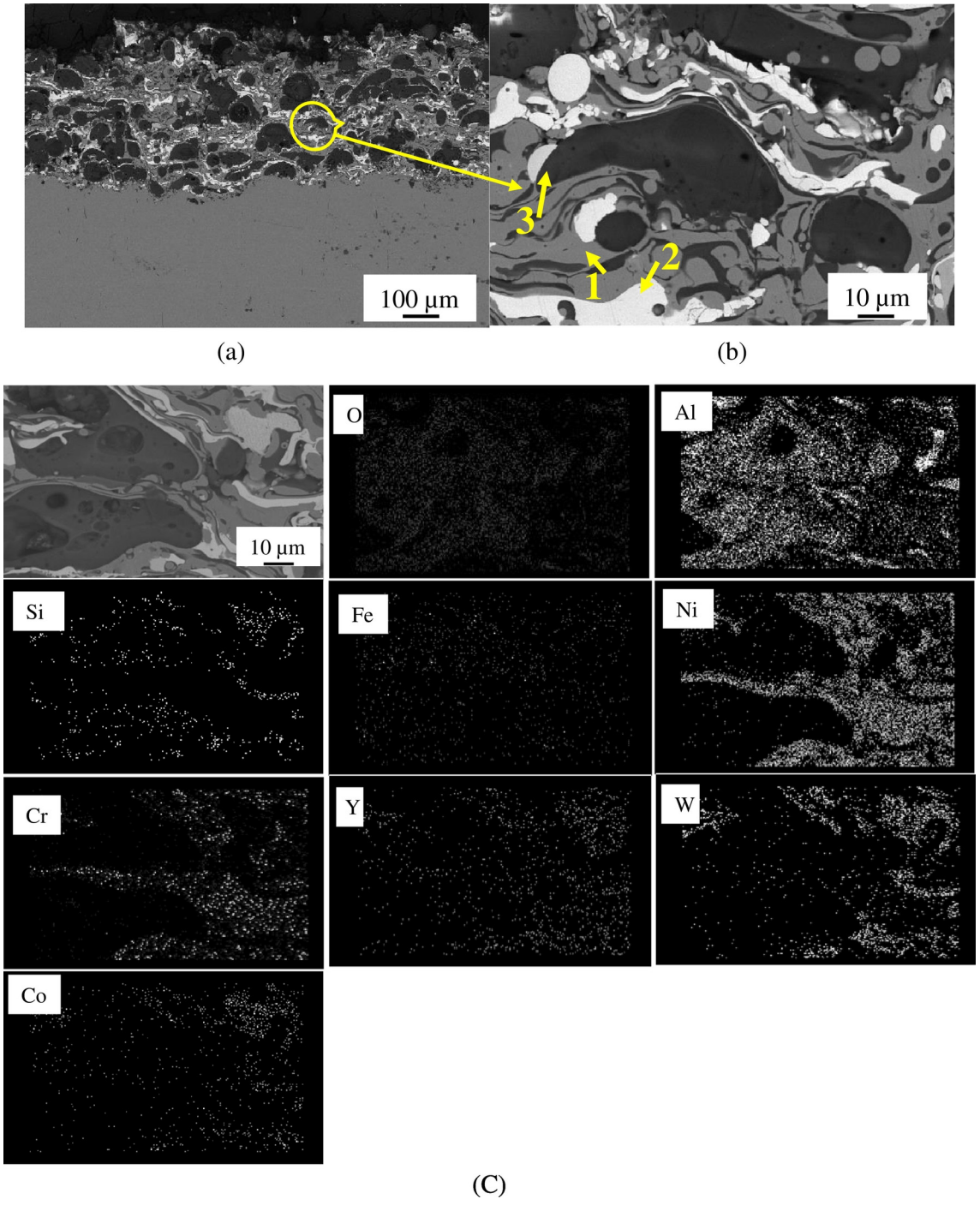

Fig. 3. Micrograph of the coating taken throughout the coating thickness and EDS elemental mapping.

Table 5
EDS analysis of coating at the designated point in Fig. 3b.

Element	Oxide	Phase 1	Phase 2	Phase 3
–	SiO_2	–	–	57.50
–	Al_2O_3	–	–	39.23
–	Fe_2O_3	–	–	3.26
Al	–	1.75	–	–
Si	–	–	–	–
C	–	–	08.43	–
Cr	–	20.27	–	–
Ni	–	77.46	–	–
Y	–	0.52	–	–
W	–	–	79.40	–
Co	–	–	12.17	–

calculated by measuring radial crack length [26] using,

$$K_{IC} = 0.0193\ (H_V d)\left(\frac{E}{H_V}\right)^{\frac{2}{5}} (a)^{-\frac{1}{2}} \ldots\ldots\ldots \left(\frac{c}{d} \le 2.5\right) \text{Palmqvist Cracks} \quad (1)$$

$$K_{IC} = 0.0711\ \left(H_V d^{\frac{1}{2}}\right)\left(\frac{E}{H_V}\right)^{\frac{2}{5}} \left(\frac{c}{d}\right)^{-\frac{3}{2}} \ldots. \left(\frac{c}{d} \ge 2.5\right) \text{Half penny Cracks} \quad (2)$$

where 'H_V' is Vickers hardness, 'E' is Young's modulus and 'd' is half-diagonal of the Vickers indentation. The radial crack length 'a' equals difference between indentation crack length 'c' and 'd'. Values of 'a', 'c' and 'd' are measured from micrographs. Vickers microhardness (OMNITECH, S-AUTO, INDIA) of coating is measured with 300 g load for 10s dwell time. Chosen test load and dwell time provides a better view of indentation in microscope to measure indentations dimension [27] on the polished transverse cross section of the coating and substrate. Samples are polished down to mirror finish using cloth polishing wheel machine with 1 μm lavigated alumina powder suspension. Average values of 10 indentations taken at different locations are reported.

2.4. Ductility

Load-displacement data acquired from nano indentation test is used to compute coating ductility. Ductility is the ratio of the plastic work, W_p to the total work, Wt [25]. W_p is obtained from the area enclosed by the loading and the unloading curve whereas area below the loading curve is represented by W_t, in load-displacement plot. Nano indentation test (Agilent, G200, USA) is carried out on polished surface of the coating for 30 g load, which is selected based on coating thickness. Coating surface is polished down to 1000 grit emery paper. Nano indentation is done at 10 different locations and average value is reported.

2.5. Erosion study

Solid particle erosion test is carried out as per ASTM G76-13 using air jet erosion tester (TR-471-800, Ducom instruments Pvt. Ltd., Bangalore, INDIA). Alumina grits are used as erodent. Schematic representation of the test setup is presented in Fig. 2. Erodent is fed to the mixing chamber at 2 g/min which gets mixed with hot air flowing through spiral tube surrounded by tubular heaters. This erodent and air mixture impinges with 30 m/s velocity on the sample which is rigidly fixed in sample holder. Erodent velocity is measured by double disc method prior to test. Specimen is heated by the heating elements arranged in the cylindrical manner surrounding the samples as depicted in Fig. 2. The impact angle is set by varying the orientation of the sample holder with respect to the erodent stream. Erosion test is conducted with the set parameters as listed in Table 4.

Prior to the erosion test, samples are cleaned in acetone, dried and clamped in the erosion setup. All the samples are subjected to the predefined temperatures for 20 min before test to simulate actual testing conditions. After each test, samples are cleaned in acetone, dried and weighed using electronic weighing balance (least count of 0.0001 g) to estimate mass loss. The erosion rate is computed by ratio of mass loss to erodent particles mass. The volume loss of the eroded samples is quantified using 3D optical non-contact profilometer (Zeta instruments, 20, USA).

3. Results and discussion

3.1. Microstructure analysis of coating

SEM micrograph of coating cross section is presented in Fig. 3. As seen from the micrograph, coating is bonded well with substrate and shows uniform dispersion of cenospheres. Average thickness of the coating observed is 350 μm (Fig. 3a) having average area porosity of 4 ± 0.3%. The circled area in Fig. 3a is enlarged and presented in Fig. 3b shows lamellar densely packed structure of NiCrAlY-25WC-Co/cenosphere coating. Constituents present in Fig. 3b are marked as 1 -

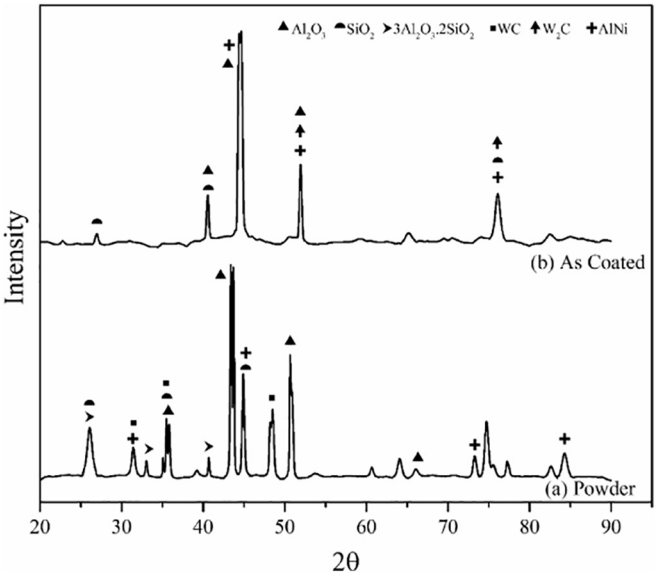

Fig. 4. X ray diffraction pattern of as (a) blended powder and (b) coated sample.

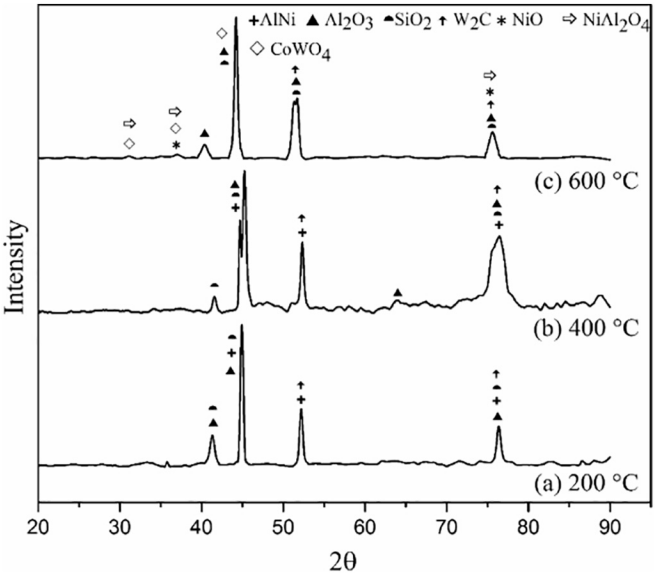

Fig. 5. X ray diffraction pattern of eroded samples at different temperatures.

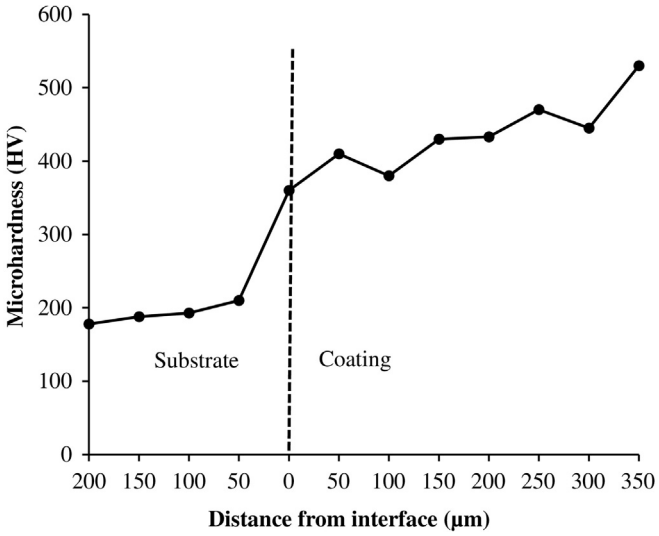

Fig. 6. Microhardness profile of substrate and coating.

NiCrAlY matrix, 2– WC-Co phase and 3 - cenosphere particles based on the EDS analysis presented in Table 5. Fig. 3c depicts elemental mapping of the coating which clearly shows distinct splats enriched with oxygen, co-exist with aluminium, silicon and iron indicating presence of respective oxides. Nickel and chromium are uniformly distributed around tungsten carbide-cobalt and cenospheres splat boundaries as seen from Fig. 3c.

3.2. XRD analysis

The X-ray diffraction pattern of blended powder and as sprayed coating is exhibited by Fig. 4. XRD pattern of blended powder consists of Al_2O_3, SiO_2 and AlNi major phases and minor phases of $3Al_2O_3$, $2SiO_2$, WC. XRD pattern of coating depicts Al_2O_3 and AlNi as major and W_2C as minor phases. Decarburization of WC during plasma spraying results in presence of W_2C. WC decomposes significantly into W_2C during spraying owing to higher temperatures in the plasma spray process.

Fig. 5 presents XRD pattern of eroded samples at 200, 400 and 600 °C. As seen from this figure similar patterns are seen at all temperatures. NiO, $NiAl_2O_4$, Al_2O_3 and $CoWO_4$ are observed at 600 °C due to oxidation. These oxides form protective layer and resist erosion at elevated temperature.

3.3. Microhardness measurement

Microhardness profile as a function of distance from coating-substrate interface is depicted by Fig. 6. The average microhardness of coating and the substrate are 428 ± 48 and 189 ± 10 HV respectively. Significant increase in microhardness across the interface is due to work hardening of substrate during grit blasting resulting from peening stresses. Microhardness of the coating is seen to be varied along the cross section due to inhomogeneity in the coating structure as seen from Fig. 3b.

3.4. Adhesion strength and indentation fracture toughness

Durability of the coatings depends on adhesion strength between the substrate and coating. Fractured surface morphology of the coating after adhesion strength test is exhibited by Fig. 7. Fracture surface reveal adhesive failure between coating and substrate interface. Adhesion strength of the coating is observed to be 8.40 MPa. Similar values of adhesion strength are reported by A. Behera and S. C. Mishra [23], Mishra et al. [28] for the plasma sprayed fly ash based composite coatings. Fracture toughness is calculated using Eq. (1) as the ratio of 'c/d' which is measured by indentation and is noted to be within the range of 1–1.6 implying existence of Palmqvist Cracks. Cracks are initiated from the indenter end and are parallel to the coating interface. The average value of fracture toughness observed in the present work is 3.10 MPa $m^{1/2}$. Similar results are reported by Avnish Kumar et al. [27] and Robert J.K. wood [29] for WC-10Co-Cr and WC-Co coatings respectively.

3.5. Ductility

Ductility of the coating is measured in binder and hard phase (Fig. 8). It varies between 0 (perfectly elastic) and 1 (perfectly plastic) [25]. W_p/W_t ratio of the coating in the binder and hard phases is 0.83 and 0.75 respectively implying better ductility. The plastic deformation of the matrix (Fig. 14a) embraced the hard particles, leading to improved erosion resistance of coating.

3.6. Erosive behavior of substrate and coating

3D profiles of eroded substrate surface tested at 600 °C with 30 and 90° impact angles are presented in Fig. 9 and shows higher erosion volume loss at 90° impact angle. Effect of temperature on the erosion rate and volume loss of the substrate is presented in Fig. 10. Erosion loss increases with increasing temperature and impact angle, more prominent being at 600 °C (Fig. 10b). Erosion loss at 600 °C is approximately 3.5 and 2.5 times higher as compared to 200 °C at 30 and 90° impact angles

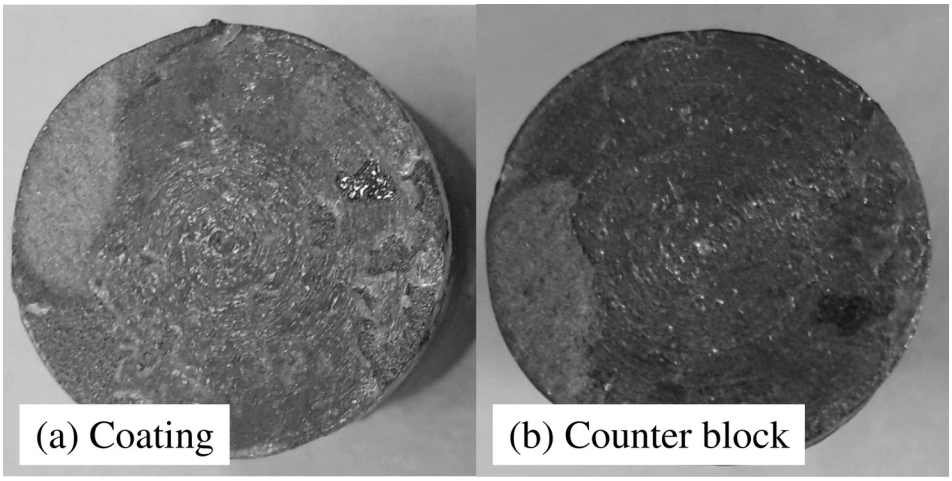

Fig. 7. Fractured surface after adhesion test in (a) coated sample and (b) counter body.

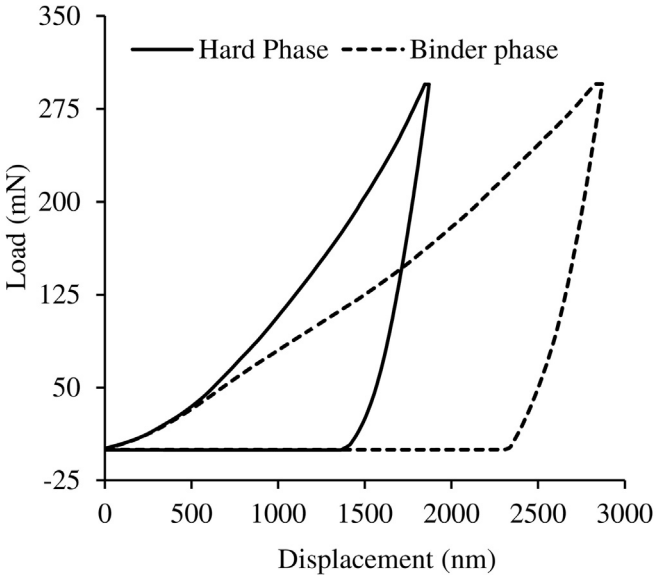

Fig. 8. Load-displacement response of hard and binder phase of coating.

respectively. Annealing effect lowers substrate hardness with rise in temperature. At higher temperature oxide layer formed is insufficient to resist erodent impact leading to cracking of oxide layer followed by its removal. Hence, increasing volume loss is noted with temperature rise.

3-D profiles of eroded coating surface at 600 °C with 30 and 90° impact angles are presented in Fig. 11. Effect of temperature on the erosion rate and volume loss is presented in Fig. 12. It is observed that erosion rate of the coating is less than the substrate at all the test temperatures. This is attributed to higher hardness and higher temperature stability of the constituents and oxidation resistance of the coating. Similar results are reported by Yang et al. [30] for Cr_3C_2-NiCr coating for boiler tube application. At 200 °C there is no significant difference in the erosion volume loss (Fig. 12b) between 30 and 90° impact angles implying neither ductile nor brittle behavior of coating. Similar results are reported by Mishra et al. [12] for plasma sprayed NiCrAlY coating at room temperature. On the contrary, at higher temperatures, i.e. at 400 and 600 °C, significant difference in volume loss is observed for both the impact angles. The erosion volume loss at 90° impact angle is higher than that at 30° implying brittle mode of erosion. Praveen et al. [31] observed the similar behavior for plasma sprayed NiCrSiB/Al_2O_3 coating tested at 450 °C. Erosion volume loss at 30° impact angle decreased with increase in test temperature. The volume loss at 600 °C is half the value as observed at 200 °C. At lower impact of 30°, an erodent particle slide on the surface and ploughs the material. Further, as the test temperature increases, material becomes soft leading to rise in ductility. Coating deforms plastically due to ductility rise and further prevents cracking in turn improving erosion resistance. At elevated temperature protective oxides like NiO, $NiAl_2O_4$ and $CoWO_4$ as seen from Fig. 5. Better erosion resistance at higher temperature under lower impact angle is due to higher coating

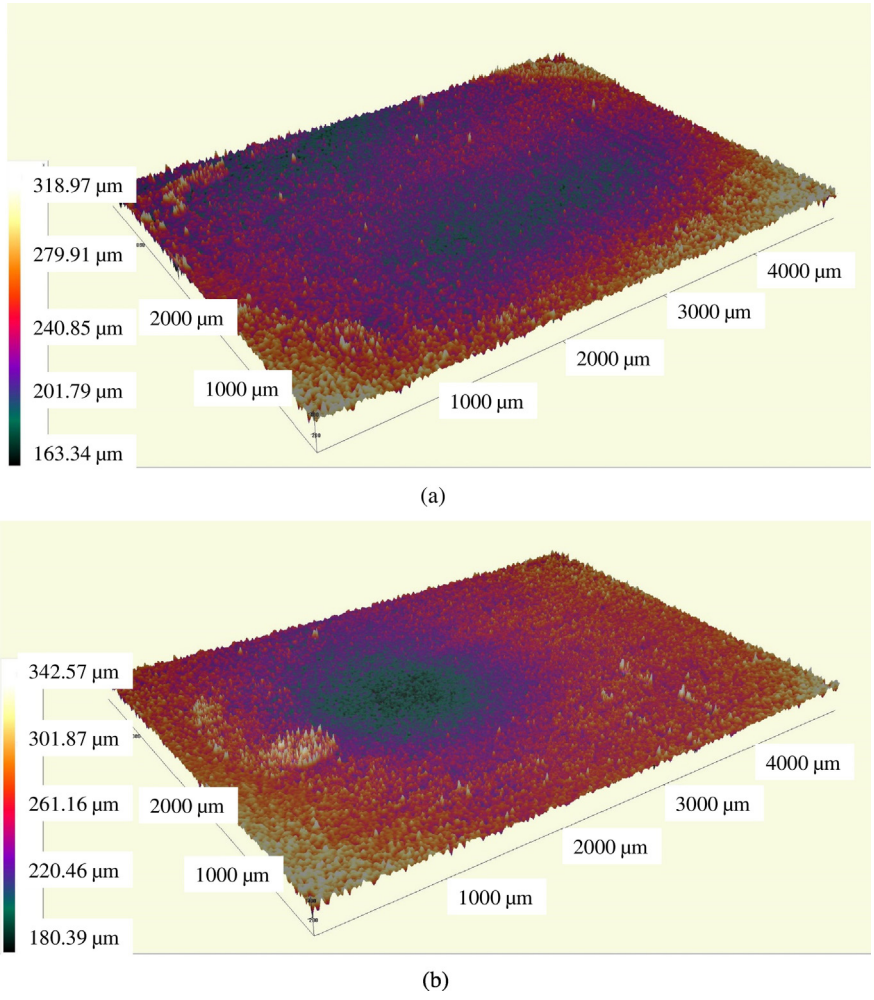

Fig. 9. Eroded profile of substrate at 600 °C with impact angles of (a) 30 and (b) 90°.

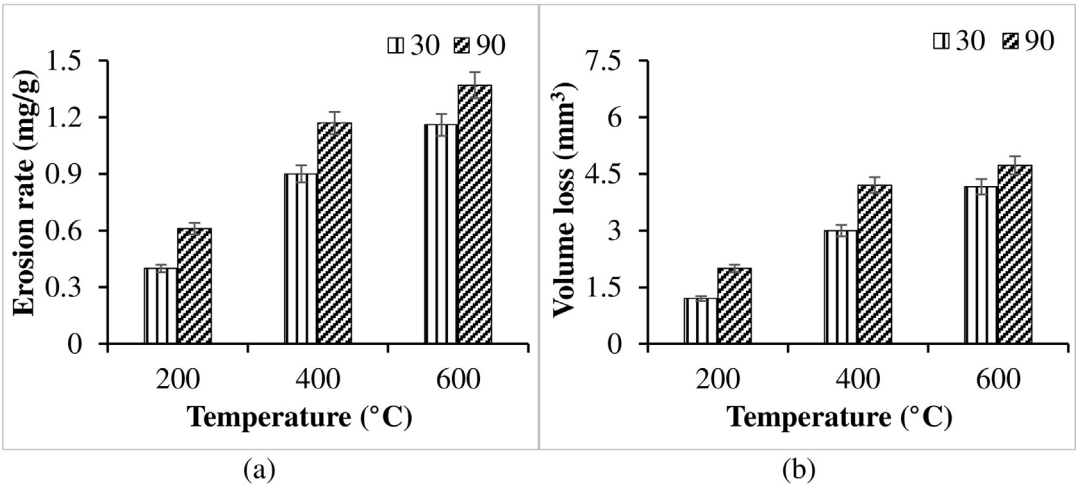

Fig. 10. Erosion rate and volume loss of substrate as function of temperature at 30 and 90° impact angles.

hardness [32]. At lower impact angle, erodent particles slide without initiating brittle cracks in the formed protective oxide layer leading to higher coating hardness. Erosion volume loss at 90° impact angle is higher at elevated temperature as the area of contact is minimum for erodent particles compare to lower impact angle. Oxide layer being brittle, fractures in fragments leading to multiple cracks. In addition, presence of W_2C phase at higher temperature leads to the embrittlement of coating surface leading to brittle mode of fracture.

Morphology of the eroded substrate surface at 600 °C with both impact angles are shown in Fig. 13. Maximum material loss takes place in ductile mechanism at lower impact angles, whereas higher impact angle governs brittle mode of material removal [33]. From Fig. 13a, it is observed that substrate undergoes severe plastic deformation leading to ploughing which forms lip towards exit end of erodent impact. With subsequent impacts, these highly strained lips are vulnerable to be removed as micro-platelets. At high temperature, hardness of the

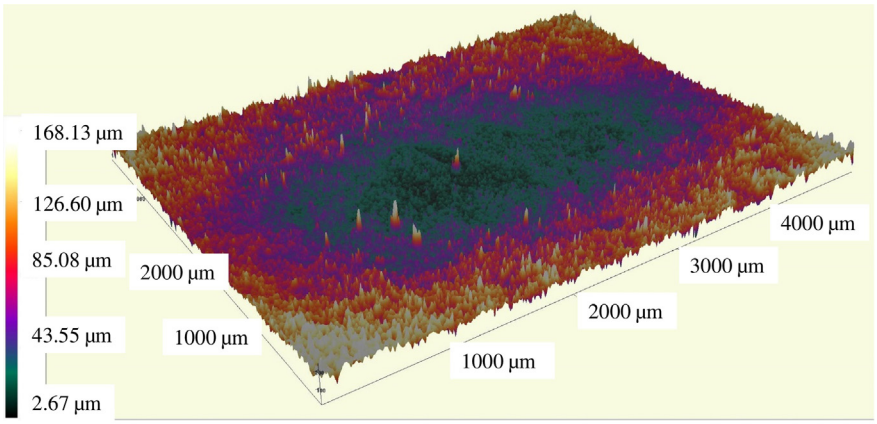

Fig. 11. 3-D profile of eroded surface of coating at 600 °C with impact angles of (a) 30 and (b) 90°.

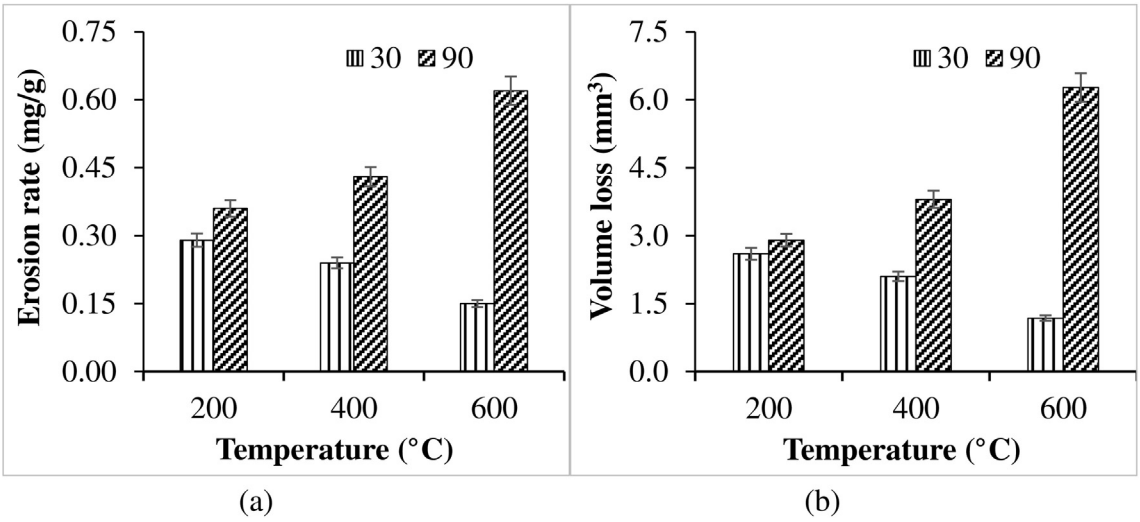

Fig. 12. Erosion rate and volume loss of coating as a function of temperature at 30 and 90° impact angles.

substrate decreases and as the erodent particle slides at lower impact angles, substrate gets deformed and subsequently removed. At normal impact angle craters are observed as seen in the micrograph (Fig. 13b). Once erodent impacts the surface, crack initiates extruding the substrate in the form of micro-platelets from the impact site. These platelets which are bonded to the crater rim are further tapped/rammed by the subsequent erodent impact and get strained to critical/threshold limit. Such highly deformed platelets are detached by subsurface crack propagation.

Fig. 14a shows the morphology of the eroded coating surface at 600 °C under 30° impact angle with number of grooves and lips indicating material removal by ploughing and microcutting. At lower impact angles, hard erodent particles slides on the surface and being in contact for a longer time leads to micro ploughing of the relatively soft binder phase. EDAX analysis (Fig. 14b) at point 1 confirms the NiCr rich binder matrix where ploughing took place. Such ploughing exposes harder particles to the erodent and subsequently gouged out by repeated hammering effect of erodent particles. This in turn initiate small cracks across the boundary of matrix and hard particles creating smaller size craters. Ramesh et al. [1] and Murthy et al. [34] reported similar pull out phenomena in WC-Co/NiCrFeSiB and WC-Co-Cr coating.

Fig. 15a shows the morphology of eroded coating surface at 600 °C with 90° impact angle. The maximum erosion volume loss occurred at higher impact angle implying brittle mode of material removal. Craters and cracks are observed due to strain localization leading to brittle fracture of splats. Cracks are generated at the interface of matrix and hard particles as only one-third interface area is bonded together in plasma spray coatings while remaining area acts as inter-lamellar gaps which can be treated as pre-existing cracks [35]. With progress of erosion, radial and lateral cracks are developed on the surface and sub-surface of coating. These cracks interlock with the pre-existing non bonded area and remove the lamella or lamellae. EDAX analysis (Fig. 15b) at point 1 confirms the cenosphere particle owing to presence of Al and Si oxides. Crack gets initiated at the particle boundary leading to particle removal by repetitive erodent impact.

4. Conclusion

- Plasma spraying has been successfully used to develop NiCrAlY-25WC-Co/Cenosphere coating having adhesion strength of 8.40 MPa.
- Erosion resistance of developed coating increases with increasing temperature for 30° impact angle. At elevated temperature erosion resistance of coating is 71% higher than MDN 321 steel substrate.
- Elevated temperature erosion resistance of the coating at 90° impact angle is 81% lower than 30° impact angle due to embrittlement of W_2C phase and oxide layer fragmentation.
- Coating exhibits brittle erosive mechanism irrespective of temperature, wherein material is removed by crack formation and chipping at higher impact angles.

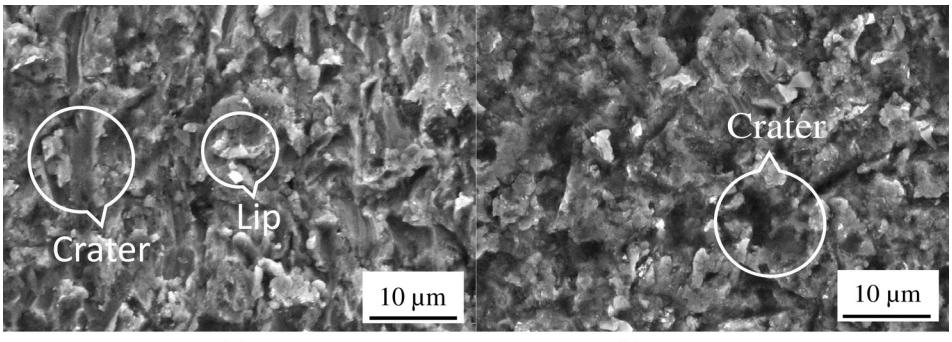

Fig. 13. SEM images of eroded surface of substrate at 600 °C with impact angles of (a) 30 and (b) 90°.

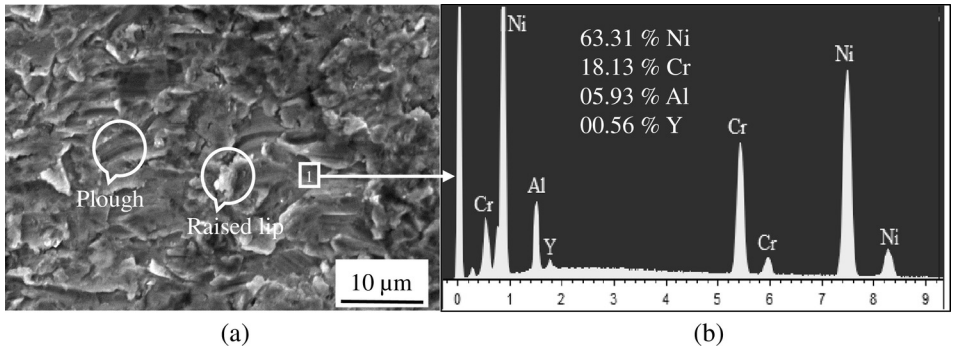

Fig. 14. (a) SEM images of eroded surface of coating at 600 °C with 30° impact angle and their (b) EDAX analysis.

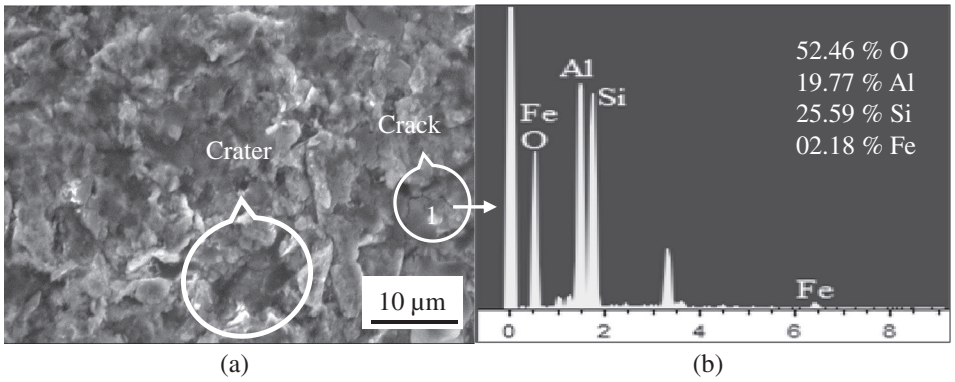

Fig. 15. (a) SEM images of eroded surface of coating at 600 °C with 90° impact angle and their (b) EDAX analysis.

Acknowledgements

The authors are grateful to Prof. Ramesh Singh, IIT Bombay, India, for providing the optical profilometer facility. The authors wish to thank Spraymet Surface technologies Pvt. Ltd., Bangalore, India, for providing the facility of the plasma spray coating. The authors thank Mechanical Engineering department at NITK Surathkal for providing support in carrying out this work. This research did not receive any specific grant from funding agencies in the public, commercial, or not-for-profit sectors.

References

[1] M.R. Ramesh, S. Prakash, S.K. Nath, P.K. Sapra, B. Venkataraman, Wear 269 (3) (2010) 197–205.
[2] S.B. Mishra, K. Chandra, S. Prakash, Surf. Coat. Technol. 216 (2013) 23–34.
[3] M. Manjunatha, R.S. Kulkarni, M. Krishna, Procedia Mater. Sci. 2014 (5) (2014) 622–629.
[4] G. Bolelli, I. Hulka, H. Koivuluoto, L. Lusvarghi, A. Milanti, K. Niemi, P. Vuoristo, Surf. Coat. Technol. 247 (2014) 74–89.
[5] J.B. Cheng, X.B. Liang, Y.X. Chen, Z.H. Wang, B.S. Xu, J. Therm. Spray Technol. 22 (5) (2013) 820–827.
[6] S. Sharma, J. Insti. Eng. (India) Ser. D. 93 (1) (2012) 7–12.
[7] V. Bonache, M.D. Salvador, J.C. García, E. Sánchez, E. Bannier, J. Therm. Spray Technol. 20 (3) (2011) 549–559.
[8] L. Du, C. Huang, W. Zhang, T. Li, W. Liu, Surf. Coat. Technol. 205 (12) (2011) 3722–3728.
[9] C. Huang, L. Du, W. Zhang, Surf. Coat. Technol. 203 (20) (2009) 3058–3065.
[10] S.B. Mishra, K. Chandra, S. Prakash, B. Venkataraman, Surf. Coat. Technol. 201 (3) (2006) 1477–1487.
[11] X. Ren, F. Wang, Surf. Coat. Technol. 201 (1) (2006) 30–37.
[12] S.B. Mishra, K. Chandra, S. Prakash, Mater. Lett. 62 (12) (2008) 1999–2002.
[13] S.B. Mishra, K. Chandra, S. Prakash, Surf. Coat. Technol. 216 (2013) 23–34.
[14] G. Bolelli, A. Candeli, L. Lusvarghi, A. Ravaux, K. Cazes, A. Denoirjean, S. Valette, C. Chazelas, E. Meillot, L. Bianchi, Wear 344 (2015) 69–85.
[15] H.S. Grewal, H. Singh, A. Agrawal, Surf. Coat. Technol. 216 (2013) 78–92.
[16] M. Jafari, M.H. Enayati, M. Salehi, S.M. Nahvi, C.G. Park, Mater. Sci. Eng. A 578 (2013) 46–53.
[17] V. Manakari, G. Parande, M. Doddamani, V.N. Gaitonde, I.G. Siddhalingeshwar, V.C. Shunmugasamy, N. Gupta, Tribol. Int. 92 (2015) 425–438.
[18] A. Arizmendi-Morquecho, A. Chávez-Valdez, J. Alvarez-Quintana, Appl. Therm. Eng. 48 (2012) 117–121.
[19] S. Das, S. Ghosh, A. Pandit, T.K. Bandyopadhyay, A.B. Chattopadhyay, K. Das, J. Mater. Sci. 40 (18) (2005) 5087–5089.
[20] S.C. Mishra, K.C. Rout, P.V. Padmanabhan, B. Mills, J. Mater. Process. Technol. 102 (1) (2000) 9–13.
[21] L.R. Krishna, D. Sen, D.S. Rao, G. Sundararajan, J. Therm. Spray Technol. 12 (1) (2013) 77–79.
[22] B.S. Sidhu, H. Singh, D. Puri, S. Prakash, Tribol. Int. 40 (5) (2007) 800–808.
[23] S.P. Sahu, A. Satapathy, A. Patnaik, K.P. Sreekumar, P.V. Ananthapadmanabhan, Mater. Des. 31 (3) (2010) 1165–1173.
[24] A. Behera, S.C. Mishra, National Seminar on Waste to Wealth Organized by Indian Institute off Metals-Bhubaneswar Chapter and SGAT-Bhubaneswar, 2012.
[25] J.K.N. Murthy, K.S. Prasad, K. Gopinath, B. Venkataraman, Surf. Coat. Technol. 204 (24) (2010) 3975–3978.
[26] A. Mateen, G.C. Saha, T.I. Khan, F.A. Khalid, Surf. Coat. Technol. 206 (6) (2011) 1077–1084.
[27] A. Kumar, A. Sharma, S.K. Goel, Appl. Surf. Sci. 370 (2016) 418–426.
[28] S.C. Mishra, A. Satapathy, K.P. Singh, S. Sethy, P.V. Padmanabhan, K.P. Sreekumar, R. Satpute, Proceedings of the International Seminar on Mineral Processing Technology, Chennai, 2010 825–829.
[29] R.J.K. Wood, Int. J. Refract. Met. Hard Mater. 28 (1) (2010) 82–94.
[30] G.J. Yang, C.J. Li, S.J. Zhang, C.X. Li, J. Therm. Spray Technol. 17 (5–6) (2008) 782–787.
[31] A.S. Praveen, J. Sarangan, S. Suresh, J.S. Subramanian, Int. J. Refract. Met. Hard Mater. 52 (2015) 209–218.
[32] P. Kulu, T. Pihl, J. Therm. Spray Technol. 11 (4) (2002) 517.
[33] C.S. Ramachandran, V. Balasubramanian, P.V. Ananthapadmanabhan, Ceram. Int. 39 (1) (2013) 649–672.
[34] J.K.N. Murthy, D.S. Rao, B. Venkataraman, Wear 249 (7) (2001) 592–600.
[35] G.C. Ji, C.J. Li, Y.Y. Wang, J. Therm. Spray Technol. 16 (4) (2007) 557–565.